



Optimization of the first CUPID detector module

CUPID Collaboration^{7,a}, K. Alfonso^{1,2}, A. Armatol³, C. Augier⁴, F. T. Avignone III⁵, O. Azzolini⁶, M. Balata⁷, A. S. Barabash⁸, G. Bari⁹, A. Barresi^{10,11}, D. Baudin³, F. Bellini^{12,13}, G. Benato⁷, M. Beretta¹⁴, M. Bettelli¹⁵, M. Biassoni¹⁰, J. Billard⁴, V. Boldrini^{9,15}, A. Branca^{10,11}, C. Brofferio^{10,11}, C. Bucci⁷, J. Camilleri¹, A. Campani^{16,17}, C. Capelli¹⁸, S. Capelli^{10,11}, L. Cappelli⁷, L. Cardani¹², P. Carniti^{10,11}, N. Casali¹², E. Celi^{7,19}, C. Chang²⁰, D. Chiesa^{10,11}, M. Clemenza¹⁰, I. Colantoni^{12,21}, S. Copello^{16,17}, E. Craft²², O. Cremonesi¹⁰, R. J. Creswick⁵, A. Cruciani¹², A. D'Addabbo⁷, G. D'Imperio¹², S. Dabagov²³, I. Dafinei¹², F. A. Danevich²⁴, M. De Jesus⁴, P. de Marcillac²⁵, S. Dell'Oro^{10,11}, S. Di Domizio^{16,17}, S. Di Lorenzo⁷, T. Dixon^{3,25}, V. Dompè^{12,13}, A. Drobizhev¹⁸, L. Dumoulin²⁵, G. Fantini^{12,13}, M. Faverzani^{10,11}, E. Ferri¹⁰, F. Ferri³, F. Ferroni^{26,19}, E. Figueroa-Feliciano²⁷, L. Foggetta²³, J. Formaggio²⁸, A. Franceschi²³, C. Fu²⁹, S. Fu^{29,7}, B. K. Fujikawa¹⁸, A. Gallas²⁵, J. Gascon⁴, S. Ghislandi^{7,19}, A. Giachero^{10,11}, A. Gianvecchio^{10,11}, L. Gironi^{10,11}, A. Giuliani²⁵, P. Gorla⁷, C. Gotti¹⁰, C. Grant³⁰, P. Gras³, P. V. Guillaumon⁷, T. D. Gutierrez³¹, K. Han³², E. V. Hansen¹⁴, K. M. Heeger²², D. L. Helis^{7,19}, H. Z. Huang^{2,29}, L. Imbert²⁵, J. Johnston²⁸, A. Juillard⁴, G. Karapetrov³³, G. Keppel⁶, H. Khalife³, V. V. Kobaychev²⁴, Yu. G. Kolomensky^{14,18}, S. I. Konovalov⁸, R. Kowalski³⁴, T. Langford²², M. Lefevre³, R. Liu²², Y. Liu³⁵, P. Loaiza²⁵, L. Ma²⁹, M. Madhukuttan²⁵, F. Mancarella^{9,15}, L. Marini^{7,19}, S. Marnieros²⁵, M. Martinez^{36,37}, R. H. Maruyama²², Ph. Mas³, B. Mauri³, D. Mayer²⁸, G. Mazzitelli²³, Y. Mei¹⁸, S. Milana¹², S. Morganti¹², T. Napolitano²³, M. Nastasi^{10,11}, J. Nikkel²², S. Nisi⁷, C. Nones³, E. B. Norman¹⁴, V. Novosad²⁰, I. Nutini^{10,11}, T. O'Donnell¹, E. Olivieri²⁵, M. Olmi⁷, J. L. Ouellet²⁸, S. Pagan²², C. Pagliarone⁷, L. Pagnanini^{7,19}, L. Pattavina⁷, M. Pavan^{10,11}, H. Peng³⁸, G. Pessina¹⁰, V. Pettinacci¹², C. Pira⁶, S. Pirro⁷, D. V. Poda²⁵, O. G. Polischuk²⁴, I. Ponce²², S. Pozzi^{10,11}, E. Previtali^{10,11}, A. Puiu^{7,19}, S. Quitadamo^{19,7}, A. Ressa^{12,13}, R. Rizzoli^{15,9}, C. Rosenfeld⁵, P. Rosier²⁵, J. Scarpaci²⁵, B. Schmidt^{18,27}, V. Sharma¹, V. N. Shlegel³⁹, V. Singh¹⁴, M. Sisti¹⁰, P. Slocum²², D. Speller³⁴, P. T. Surukuchi²², L. Taffarello⁴⁰, C. Tomei¹², J. A. Torres²², V. I. Tretyak²⁴, A. Tsymbaliuk⁶, M. Velazquez⁴¹, K. J. Vetter¹⁴, S. L. Wagaarachchi¹⁴, G. Wang²⁰, L. Wang³⁵, R. Wang³⁴, B. Welliver^{14,18}, J. Wilson⁵, K. Wilson⁵, L. A. Winslow²⁸, M. Xue³⁸, L. Yan²⁹, J. Yang³⁸, V. Yefremenko²⁰, V. I. Umatov⁸, M. M. Zarytskiy²⁴, J. Zhang²⁰, A. Zolotarova³, S. Zucchelli^{9,42}

¹ Virginia Polytechnic Institute and State University, Blacksburg, VA, USA

² University of California, Los Angeles, CA, USA

³ IRFU, CEA, Université Paris-Saclay, Saclay, France

⁴ Univ Lyon, Université Lyon 1, CNRS/IN2P3, IP2I-Lyon, 69622 Villeurbanne, France

⁵ University of South Carolina, Columbia, SC, USA

⁶ INFN Laboratori Nazionali di Legnaro, Legnaro, Italy

⁷ INFN Laboratori Nazionali del Gran Sasso, Assergi, AQ, Italy

⁸ National Research Centre Kurchatov Institute, Institute for Theoretical and Experimental Physics, Moscow, Russia

⁹ INFN Sezione di Bologna, Bologna, Italy

¹⁰ INFN Sezione di Milano-Bicocca, Milan, Italy

¹¹ University of Milano-Bicocca, Milan, Italy

¹² INFN Sezione di Roma, Rome, Italy

¹³ Sapienza University of Rome, Rome, Italy

¹⁴ University of California, Berkeley, CA, USA

¹⁵ CNR-Institute for Microelectronics and Microsystems, Bologna, Italy

¹⁶ INFN Sezione di Genova, Genoa, Italy

¹⁷ University of Genova, Genoa, Italy

¹⁸ Lawrence Berkeley National Laboratory, Berkeley, CA, USA

¹⁹ Gran Sasso Science Institute, L'Aquila, Italy

²⁰ Argonne National Laboratory, Argonne, IL, USA

²¹ CNR-Institute of Nanotechnology, Rome, Italy

- ²² Yale University, New Haven, CT, USA
²³ INFN Laboratori Nazionali di Frascati, Frascati, Italy
²⁴ Institute for Nuclear Research of NASU, Kyiv, Ukraine
²⁵ Université Paris-Saclay, CNRS/IN2P3, IJCLab, Orsay, France
²⁶ INFN Sezione di Roma and Sapienza University of Rome, Rome, Italy
²⁷ Northwestern University, Evanston, IL, USA
²⁸ Massachusetts Institute of Technology, Cambridge, MA, USA
²⁹ Fudan University, Shanghai, China
³⁰ Boston University, Boston, MA, USA
³¹ California Polytechnic State University, San Luis Obispo, CA, USA
³² Shanghai Jiao Tong University, Shanghai, China
³³ Drexel University, Philadelphia, PA, USA
³⁴ Johns Hopkins University, Baltimore, MD, USA
³⁵ Beijing Normal University, Beijing, China
³⁶ Centro de Astropartículas y Física de Altas Energías, Universidad de Zaragoza, Zaragoza, Spain
³⁷ ARAID Fundación Agencia Aragonesa para la Investigación y el Desarrollo, Zaragoza, Spain
³⁸ University of Science and Technology of China, Hefei, China
³⁹ Nikolaev Institute of Inorganic Chemistry, Novosibirsk, Russia
⁴⁰ INFN Sezione di Padova, Padua, Italy
⁴¹ Univ. Grenoble Alpes, CNRS, Grenoble INP, SIMAP, Grenoble, France
⁴² University of Bologna, Bologna, Italy

Received: 15 February 2022 / Accepted: 18 August 2022 / Published online: 12 September 2022
 © The Author(s) 2022

Abstract CUPID will be a next generation experiment searching for the neutrinoless double β decay, whose discovery would establish the Majorana nature of the neutrino. Based on the experience achieved with the CUORE experiment, presently taking data at LNGS, CUPID aims to reach a background free environment by means of scintillating $\text{Li}_2^{100}\text{MoO}_4$ crystals coupled to light detectors. Indeed, the simultaneous heat and light detection allows us to reject the dominant background of α particles, as proven by the CUPID-0 and CUPID-Mo demonstrators. In this work we present the results of the first test of the CUPID baseline module. In particular, we propose a new optimized detector structure and light sensors design to enhance the engineering and the light collection, respectively. We characterized the heat detectors, achieving an energy resolution of $(5.9 \pm 0.2)\text{keV}$ FWHM at the Q -value of ^{100}Mo (about 3034 keV). We studied the light collection of the baseline CUPID design with respect to an alternative configuration which features gravity-assisted light detectors' mounting. In both cases we obtained an improvement in the light collection with respect to past measures and we validated the particle identification capability of the detector, which ensures an α particle rejection higher than 99.9%, fully satisfying the requirements for CUPID.

1 Introduction

The two-neutrino double β decay ($2\nu\beta\beta$) [1] is one of the rarest processes in the universe, observed only in 11 nuclides, with typical half-lives in the range between 10^{18} and 10^{24} year [2]. The precision measurements performed by several experiments allowed detailed studies of the $2\nu\beta\beta$ spectral shape to search for distortions due to beyond Standard Model processes [3–9].

An alternative mode to this process requires the emission of 2 electrons without neutrinos in the final state and is referred to as neutrinoless double β decay ($0\nu\beta\beta$). This has been first hypothesised by Furry [10] and then supported by several theoretical frameworks [11–15]. The search for this decay plays a significant role in particle physics nowadays, as its discovery would establish the Dirac or Majorana nature of the neutrino, whose experimental evidence is still missing. In the former (Dirac) case, the neutrino behaves like all the other fermions. In the latter (Majorana) case, neutrino and antineutrino coincide, giving rise to new physics processes in which the total lepton number symmetry is violated, such as the $0\nu\beta\beta$ decay [16]. This would also represent an important hint for the explanation of the matter-antimatter asymmetry in the universe [17, 18]. Several experiments have been searching for $0\nu\beta\beta$ in different nuclides with sensitivities on the half-life from 10^{24} to 10^{26} yr [19–27] but still no evidence of this decay has been found.

The next generation experiment CUPID (CUORE Upgrade with Particle IDentification) [28] aims to explore the half-life region up to 10^{27} years. CUPID will use scintillating cryogenic calorimeters, also called bolometers. These are very

^ae-mail: cupid.publications@lngs.infn.it (corresponding author)

low temperature detectors, operated at about 10 mK, whose main element is a crystal containing the isotope candidate for the $0\nu\beta\beta$ emission. The crystal's heat capacity at cryogenic temperatures allows to convert an energy release into a measurable temperature increase. The temperature variation is then turned into an electric signal by means of a cryogenic sensor, called a thermistor. This detection mechanism is the key to achieve an excellent energy resolution, about 0.2% FWHM at a few MeV of energy deposit, which is one of the fundamental ingredients to increase the experimental sensitivity to the $0\nu\beta\beta$ search. Moreover, these detectors feature a very high $0\nu\beta\beta$ containment efficiency ($\sim 80\%$) as the crystals work both as source and absorber of the decay products. The CUPID experiment is based on years of development of such technology [29,30] culminated in the CUORE (Cryogenic Underground Observatory for Rare Events) experiment [31,32]. By collecting more than 1 tonne-year of exposure in stable conditions, CUORE set a fundamental milestone for the next generation experiments searching for rare events with cryogenic calorimeters. Despite the many results achieved, CUORE is limited by the dominant background source of α particles produced by surface contaminations [33,34]. This dominant background source can be rejected by means of scintillating crystals with dual readout of light and heat signals. Indeed, at a fixed energy deposit, the light yield of α particles is quenched with respect to β/γ [35]. The particle identification represents the main innovation of the CUPID experiment, which will couple scintillating $\text{Li}_2^{100}\text{MoO}_4$ crystals to light detectors to reject α events to a negligible level. Moreover, CUPID will search for the $0\nu\beta\beta$ in the isotope ^{100}Mo which presents an important feature; indeed, its Q -value, $(3034.40 \pm 0.17)\text{keV}$ [36], lies above the last significant γ line from natural radioactivity (at 2615 keV) and this will further reduce the background level in the ROI, by mitigating the contribution due to γ s. The combination of scintillating bolometers and high Q -value $\beta\beta$ emitters was exploited by LUCIFER [37–44] and LUMINEU [45–51] as well as by the AMoRE Collaboration [52]. The experience achieved in LUCIFER and LUMINEU resulted in two demonstrators which proved the CUPID working principles: CUPID-0 [3,4,24,53–55] and CUPID-Mo [27,51,56,57]. The former used cylindrical ZnSe scintillating crystals and Ge-disk bolometers as light detectors and took data from 2017 to 2020 at Laboratori Nazionali del Gran Sasso (LNGS). CUPID-Mo operated at Laboratoire Souterrain de Modane (LSM) from early 2019 to mid 2020, proving the excellent radiopurity, energy resolution and α particles rejection achieved with cylindrical crystals of $\text{Li}_2^{100}\text{MoO}_4$ (LMO), the compound chosen for CUPID. The ongoing R&D measurements at the LNGS [58,59] and at the Canfranc laboratories [60] aim to optimize the detector features and design for the CUPID experiment. In this work we propose a new mechanical structure for the assem-

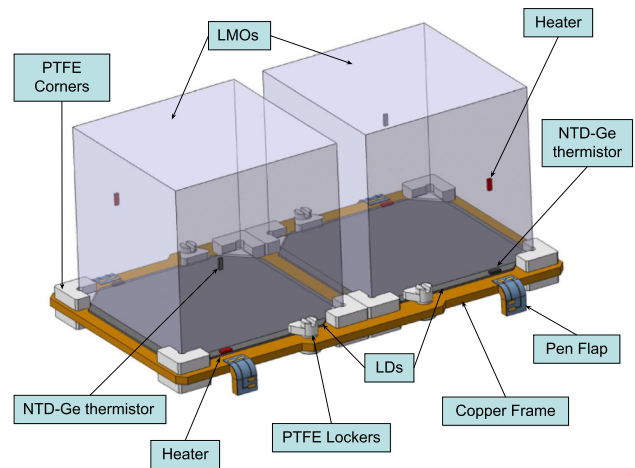


Fig. 1 Rendering of a single CUPID module which consists of 2 cubic LMO crystals and 2 LDs spaced 0.5 mm from the bottom faces. The detectors are held by the copper frame and PTFE elements. A tower is built by simply stacking one module on top of the other. The detector components are labeled in the figure

bly of the CUPID baseline detector module and present its performance.

2 Experimental setup

All the past/present bolometric detectors, from CUORE to CUPID-0 and CUPID-Mo, were assembled by mounting the crystals into copper frames, that were rigidly secured on top of each others using copper columns [44,56,61]. Experiments that featured light detectors (LDs) in their setup, usually mounted these devices by “squeezing” them into polytetrafluoroethylene (PTFE) clamps. To simplify the CUPID assembly, we designed a new mechanical structure, in which two LDs are mounted into a 2 mm thick laser-cut copper frame (Fig. 1).

Instead of squeezing the LDs in the clamps, we keep them positioned on the edges of the copper frame using two PTFE “lockers”. Furthermore, LDs were re-designed to match the CUPID crystals faces; previous measurements used CUPID-Mo [56] and CUPID-0 [62] light detectors, consisting of $170\ \mu\text{m}$ thick, disk-shaped Ge LDs. We replaced the disk-shaped LDs with quasi-square ones and, to relax the constraints on the tolerances of PTFE elements, we also increased the thickness of the LDs from 170 to $500\ \mu\text{m}$. We verified that the effect of the volume increase on the heat capacity does not affect the decay time of the pulse.

The copper frame is equipped with PTFE “corners” to ease the positioning of the LMO crystals as close as possible to the LDs (0.5 mm, largely improving the 4 mm spacing that could be achieved with the previous assembly procedure). Finally, the module design includes a pen flap, glued on the copper

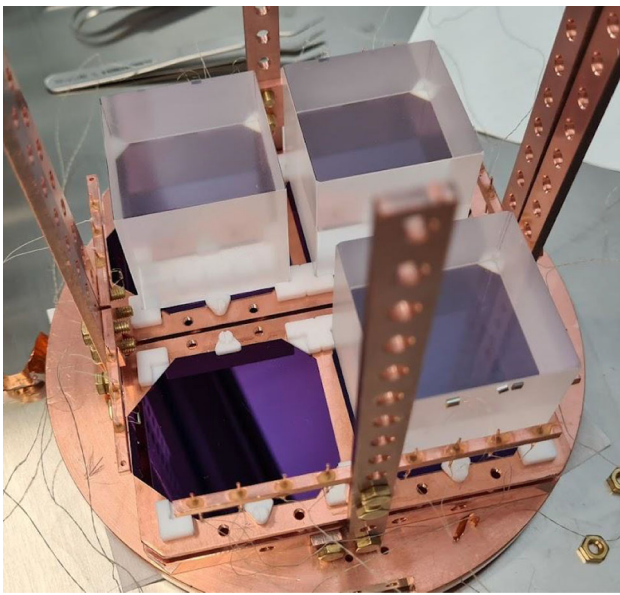


Fig. 2 Photo of the array during the decommissioning. Here are shown 2 baseline modules of CUPID, which form the first floors of the 2 mini-towers. In one of the 2 modules an LMO crystal is missing and a quasi-square LD is visible on the bottom

frame, to allow the bonding of Neutron Transmutation Doped germanium (NTD-Ge [63]) thermistors and the heaters (P-doped Si [64]). The former are meant for the read-out of both the LMO crystals and LDs, and produce a typical voltage signal of 10–100 μV per 1 MeV of deposited energy. The latter are used to periodically inject thermal pulses at a fixed energy for the thermal gain correction [61].

A CUPID tower will consist of 14 modules stacked on top of each others simply by gravity. This structure shows several advantages: it minimizes the amount of inert material, relaxes the constraints on mechanical tolerances, simplifies the production of copper elements and their cleaning, and also the assembly is simplified as well. On the other hand, such novel design was never tested before, so the thermal properties and the propagation of noise across the floors of the tower needed to be characterized. Furthermore, the novel assembly of the LDs could potentially induce a larger noise, due to a less firm positioning of the detector module components with respect to previous assemblies. In this work we made an exploratory study of the new mechanical structure, by mounting 2 mini-towers of only 2 (out of 14) floors each (Fig. 2).

Each floor hosted 2 natural LMO cubic crystals, with dimensions $45 \times 45 \times 45 \text{ mm}^3$ and mass $\sim 280 \text{ g}$ each, for a total of 8 crystals with the same specifications foreseen for CUPID. High radiopurity copper and PTFE elements were selected for the mechanical structure. Each crystal faces 2 LDs, on top and bottom. These are thin cryogenic germanium calorimeters. An antireflecting 60 nm thick layer of SiO [65]

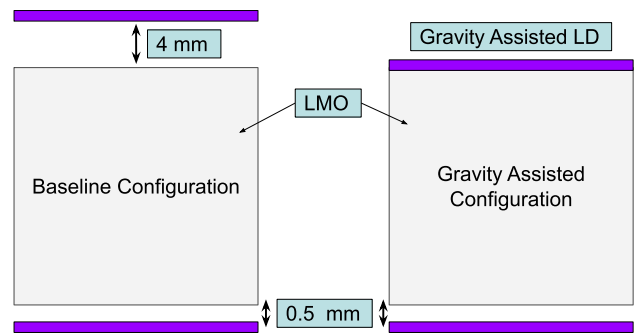


Fig. 3 Schematic view of the 2 LD configurations: the grey squares and the purple strips represent respectively the LMO crystals and the LDs. Left: “baseline” configuration with LDs spaced 0.5 and 4 mm from the bottom and top of the crystal respectively. Right: “gravity-assisted” configuration with LDs spaced 0.5 mm on bottom and leaned on top of the crystal

was deposited on both sides of the Ge faces to increase the light collection, as already done in CUPID-Mo [56]. This is the most reliable technology to be operated at cryogenic temperatures to detect scintillation light from the crystals, which typically corresponds to an equivalent deposition of keV per MeV of energy deposit in the crystal [49, 51, 56, 58, 66].

We tested 2 possible configurations of the LDs as outlined in Fig. 3:

- in the first floor, LDs were spaced 0.5 and 4 mm from the bottom and top of the crystal respectively. From now on, we will refer to this configuration as the “baseline” configuration for the CUPID experiment, as it allows a simple engineering of a large modular array.
- in the second floor, the bottom LDs were again spaced 0.5 mm, but the top LDs were leaned on the LMO crystals. This “gravity-assisted” positioning, originally proposed in Ref. [67], could allow to further increase the light collection.

One of the goals of this measurement was to establish if the larger light collection which could be offered by the “gravity-assisted” configuration is worth the complication in the detector engineering and assembly. Indeed, leaned LDs are difficult to implement on a large scale experiment with a proper assembly reproducibility.

We performed two experimental runs, one in the configuration described above, and the second one by surrounding the crystals with a Vikuiti™ reflecting foil. The latter would complicate the assembly in view of CUPID, it would be an additional source of background and it would affect the efficiency of coincidence tagging of α events. Thus we consider the reflecting foil only as a potential back-up solution to further enhance the light collection (see [58]).

The LDs were constantly exposed to an X-rays source (^{55}Fe , which produces peaks at 5.9 and 6.4 keV) to energy-

calibrate the scintillation light signals. The prototype was operated in a wet cryostat located in the Hall C of the deep underground Laboratori Nazionali del Gran Sasso of INFN, Italy.

3 Data analysis

The voltage signals from the detectors were amplified and filtered with a 120 dB/decade, six-pole anti-aliasing active Bessel filter [68–74]. We used a custom DAQ software package to save on disk the data stream acquired through a 18 bit analog-to-digital board with a sampling frequency of 2 kHz [75]. Then, a derivative trigger [76] was applied to the data, to identify thermal pulses, and a random trigger was fired every 60 s to sample the noise waveforms. The trigger parameters were tuned for each detector to optimize the noise level. We acquired heat and light pulses with a 5 s and 0.5 s long window respectively.

The triggered data were then processed offline via a dedicated analysis chain, which was adapted from a C++ based analysis framework developed for CUORE [33], CUPID-0 [77] and their predecessors [78]. The first step of the analysis was the application of a matched filter algorithm (optimum filter) [79, 80] to enhance the signal-to-noise ratio suppressing the most intense noise frequencies. This algorithm takes as input an average pulse and an average noise power spectrum, computed from recorded signal and noise waveforms, after a quality selection cut. The filter allows to improve the reconstruction of the basic pulse characteristics such as the amplitude, the baseline value (which is a proxy for the temperature), the baseline RMS and the pulse shape parameters. The filter was applied to both LD and LMO events.

Any time the trigger of an LMO crystal fired, the waveform of the corresponding LDs was acquired and flagged as “side pulses”. We exploited the fixed time delay between light and heat pulses due to the electronics in order to improve the estimate of the side pulses amplitude, which presents a poor signal-to-noise ratio at low energies. We estimated this fixed time delay for each LD from the average pulse corresponding to each channel and we evaluated the light pulses amplitude at the exact time delay with respect to the corresponding heat pulse. This allows to remove some non-linearities introduced by the optimum filter at low energies, while it does not affect significantly the light signals amplitude in the region of interest (ROI) [77].

The light signals amplitudes were energy-calibrated by using a linear function with zero intercept. The calibration coefficient was derived by fitting the peaks at 5.9 and 6.4 keV of the ^{55}Fe source.

Concerning the heat channel, a further improvement of the pulses amplitude estimation was possible through a thermal gain correction. Unlike the LDs, which exhibit typical

resolutions of $\sim 1\%$ [60], the heat channels are expected to reach a resolution of a few $\sim 0.1\%$. Such energy resolution could be spoiled by thermal instabilities of the cryostat. During the data taking we placed a ^{232}Th source outside the cryostat to derive the amplitude vs. temperature dependence in the highest energy peak from ^{208}Tl at 2615 keV, and correct the pulse amplitude accordingly. Finally, to convert the corrected amplitudes into energy, we identified and fitted the most intense mono-energetic peaks from the ^{232}Th decay chain. Then, we calibrated the heat signals by using a second order polynomial function crossing the origin, which showed residuals lower than ~ 1 keV in absolute value.

4 General performances

The temperature at which we operated the detectors of the array is ~ 15 mK. The results presented in this paper are focused on the LDs which showed the best performances. We discarded 2 LDs for reasons related to the wiring and the ^{55}Fe source placement, which are not relevant in view of CUPID. We operated the LDs with working resistances in the range of 4–7 M Ω , to obtain a response spanning from 0.9 to 5.2 $\mu\text{V}/\text{keV}$ (average ~ 2.7 $\mu\text{V}/\text{keV}$), depending on the bias current.

We evaluated the baseline RMS from a Gaussian fit to the energy spectrum of noise events and found a result between 35 and 70 eV with an average of (57 ± 6) eV, well below the threshold required for CUPID (100 eV) [28].

We did not find any correlation between the LD performance and its position in the tower. This confirms the homogeneity of the cooling along the tower and the uniformity of the results among the different LDs assembly methods. The validation of the new detector structure used in this measurement is the first important result towards the successful construction of a 14-floor tower prototype for the CUPID experiment.

We operated the LMO crystals with working resistances of 2–13 M Ω and we measured the response to be in the range of 31–72 $\mu\text{V}/\text{MeV}$ (average ~ 50 $\mu\text{V}/\text{MeV}$). We evaluated the baseline resolution as done for the LDs, with a result between 0.52 and 0.95 keV RMS depending on the LMO detector, with an overall average of (0.69 ± 0.06) keV RMS. The obtained performance is in agreement with previous cubic LMO detectors tested in the same facility [58] and consistent with cylindrical and cubic LMO detectors operated in similar conditions [49, 56, 60]. We didn't observe any significant correlation between LMO detectors performances and the kind of configuration it belongs to (“baseline” or “gravity-assisted”).

We evaluated the energy resolution at different energies by fitting the most intense γ peaks in the sum spectrum of the 8 LMO crystals (Fig. 4).

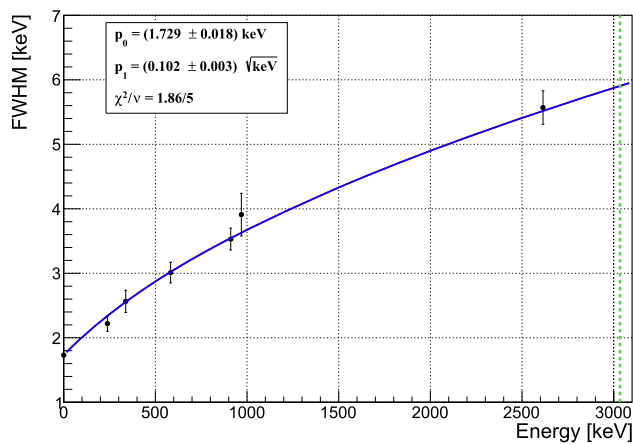


Fig. 4 FWHM of the most intense γ peaks as a function of the energy in the sum spectrum of the 8 LMO crystals. We find that the function which best describes the data is $\text{FWHM} = \sqrt{p_0^2 + p_1^2} \times E$, here shown with a blue line. The green dotted line represents the ^{100}Mo Q -value

We find a resolution of (5.6 ± 0.3) keV FWHM at the 2615 keV ^{208}Tl γ -peak. To extrapolate the energy resolution at the $Q_{\beta\beta}$ of ^{100}Mo (3034 keV), we performed different tests to evaluate the best function to describe the energy dependence of the energy resolution. We find that a square root function with a linear dependence on energy, namely $\sqrt{p_0^2 + p_1^2} \times E$, is the best fit to the data (Fig. 4). We also included in the fit the baseline resolution estimated on noise events from the overall spectrum, to better constrain the p_0 parameter. The extrapolated FWHM at the $Q_{\beta\beta}$ of ^{100}Mo is (5.9 ± 0.2) keV, which corresponds to a percentage resolution of 0.19%. The improved signal-to-noise ratio, due to an extensive characterization of the noise sources of this facility, allowed us to improve the energy resolution compared to the previous tests [58], approaching the final CUPID goal of 5 keV FWHM.

5 Light collection results

One of the main purposes of the run was the evaluation of the light collection of quasi-square light detectors and a comparison of the results obtained with different spacing between LDs and crystals. To estimate the total light collection, we added the corresponding light amplitude of top and bottom LDs and divided by the energy estimated from the heat channel. The total light yield (LY) is then calculated as the mean of the resulting distribution.

We report the total LY as a function of energy for two crystals representative of the two configurations (baseline and gravity-assisted) in Fig. 5. The results obtained with the other crystals of the respective configuration are very similar, with differences smaller than 20%.

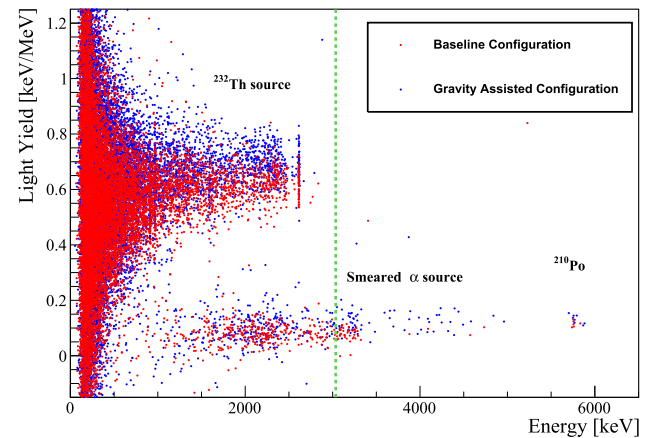


Fig. 5 Light Yield as a function of the energy deposited in the LMO crystal. Red: baseline configuration; blue: gravity-assisted configuration. Green vertical line: Q -value of ^{100}Mo

In both configurations we can clearly identify the β/γ events, which populate the plot up to the ^{208}Tl γ -line at 2615 keV, and the α events, which present a quenched light yield and extend up to higher energies. In particular, we identify a cluster of events due to an internal crystal contamination in ^{210}Po (^{210}Pb) [47], which produces a peak with nominal energy ~ 5.4 MeV. Since the detector was energy-calibrated using gamma's, the α peak is observed at slightly higher electron-equivalent energy (+ 7%, in agreement with previous studies with lithium molybdate bolometers [42, 48, 49, 56, 81]). The α events at lower energies are produced by a $^{234}\text{U}/^{238}\text{U}$ source placed in the inner face of the copper shield surrounding the detector and covered with a thin Mylar foil to smear the energy of α particles, to study the light collection in the ROI for the $0\nu\beta\beta$ search. The LY distribution shows a spread at very low energies due to the superposition of the noise with the light pulses. For this reason, to avoid the impact of noise on the LY estimation, we selected scintillation events with energy deposit in the crystal above 1.2 MeV.

The average total LY $_{\beta/\gamma}$ is found to be (0.62 ± 0.04) keV/MeV and (0.70 ± 0.05) keV/MeV in the “baseline” configuration and in the “gravity-assisted” configuration, respectively.

In particular, for the “baseline” configuration, the LYs of a single LD resulted to be on average (0.28 ± 0.02) keV/MeV for the LD spaced 4 mm and (0.33 ± 0.03) keV/MeV for the LD spaced 0.5 mm. In the “gravity-assisted” configuration we found the LY of a single LD to be (0.36 ± 0.03) keV/MeV for both the LDs. More details on the LYs of a single LD are reported in Table 1.

The total LY for α particles resulted to be (0.08 ± 0.03) keV/MeV for the “baseline” configuration and (0.11 ± 0.03) keV/MeV for the “gravity-assisted” one.

We repeated the same study on the prototype in which the LMO crystals were surrounded by reflecting foils, obtaining

Table 1 Light yield for LD top (t), LD bottom (b) and the sum of the two light detectors in the case of bare crystals. LMO-1 to LMO-4 are in the baseline configuration (bottom LD spaced 0.5 mm and top LD spaced 4 mm). LMO-5 to LMO-8 are in the “gravity assisted” configuration (bottom LD spaced 0.5 mm and top LD leaned on crystal). The missing values correspond to LDs we discarded for the analysis (LMO-1 top LD corresponds to LMO-5 bottom LD). The associated uncertainty is the width of the LY distribution

	LY _{β/γ} (t) [keV/MeV]	LY _{β/γ} (b) [keV/MeV]	LY _{β/γ} (sum) [keV/MeV]
LMO-1	–	0.35 ± 0.06	–
LMO-2	0.29 ± 0.04	0.33 ± 0.04	0.62 ± 0.06
LMO-3	0.26 ± 0.04	–	–
LMO-4	0.30 ± 0.04	0.32 ± 0.05	0.63 ± 0.06
LMO-5	0.38 ± 0.05	–	–
LMO-6	0.35 ± 0.08	0.35 ± 0.06	0.69 ± 0.09
LMO-7	0.34 ± 0.05	0.35 ± 0.04	0.69 ± 0.07
LMO-8	0.36 ± 0.07	0.37 ± 0.04	0.74 ± 0.09

in both the configurations an increase of the LY by a factor 2, as already found in Ref. [58].

From these results we conclude that the increased complexity in engineering and mounting the LDs in the “gravity-assisted” configuration is not motivated by a substantial gain in the light collection performance. For this reason, we decided to discard the “gravity-assisted” configuration in view of CUPID and from now on we will focus on the “baseline” configuration.

To quantify the particle identification capabilities of the baseline configuration, we define the Discrimination Power (DP) [82] as:

$$DP \equiv \frac{|LY_{\beta/\gamma} - LY_{\alpha}|}{\sqrt{\sigma_{\beta/\gamma}^2 + \sigma_{\alpha}^2}}. \quad (1)$$

We find that the DP for the sum of LDs ranges between 7.3 and 8.2, thus largely exceeding the requirements of CUPID. Indeed, the minimum DP needed to reject the 99.9% of α particles is 3.1 (see [28]). In the unlikely event of a loss of a light detector, the DP would diminish. Assuming that a single LD is working, we obtain a DP between 3.9 and 6.2, thus closer but still higher than the required threshold. It is worth noticing, in this context, that in the assembly of the CUORE detector only 4 out of 988 contacts were lost and that in the CUPID-0 detector none of the ~ 30 LDs exhibited any malfunction.

We report in Table 2 the DP values achieved with a single LD or with the pair of LDs in both the configurations we studied.

Finally, we compared our results with the R&D test made on disk-shaped LDs and cubic LMO crystals in the same facility [58]. To allow a coherent comparison, we consid-

Table 2 Discrimination Power (DP) achieved with the top LD (t), the bottom LD (b) and the sum of the two light detectors with bare crystals. LMO-1 to LMO-4 are in the baseline configuration (bottom LD spaced 0.5 mm and top LD spaced 4 mm). LMO-5 to LMO-8 are in the “gravity assisted” configuration (bottom LD spaced 0.5 mm and top LD leaned on crystal). The missing values correspond to LDs we discarded for the analysis (LMO-1 top LD corresponds to LMO-5 bottom LD)

	DP (t)	DP (b)	DP (sum)
LMO-1	–	3.9	–
LMO-2	5.7	6.2	8.2
LMO-3	4.4	–	–
LMO-4	5.5	4.5	7.3
LMO-5	5.7	–	–
LMO-6	3.3	4.2	5.3
LMO-7	4.3	5.9	7.4
LMO-8	3.5	6.8	5.9

ered the results obtained with the “baseline” configuration, in which the spacing between the LDs and the LMOs was similar to the assembly used in the previous test. The LY calculated from the light collected by both top and bottom LDs shows an average improvement of about 26%. This factor is consistent with the improvement expected from increasing the geometrical size of the detector ($\sim 27\%$).

6 Summary and conclusions

In view of the CUPID experiment, we modified the detector design to optimize its engineering and improve the light collection efficiency.

We validated the assembly of the new detector structure, which did not show any temperature gradient throughout the setup. This is a first fundamental step towards the construction of the 14-floor prototype tower of CUPID, which is planned for the first half of 2022.

We achieved a baseline resolution of (0.69 ± 0.06) keV RMS for the LMO crystals and we estimated an energy resolution of (5.9 ± 0.2) keV FWHM at the Q -value of ^{100}Mo (3034 keV). We reached to improve the energy resolution with respect to what reported in [58] thanks to a debug of the noise (both vibrational and electrical) of the facility and to a lower (~ 15 mK instead of ~ 18 mK) and more stable working temperature operation. We foresee that an even lower temperature (down to about ~ 11 mK as done for CUORE [32]) and an optimized electronic system will further improve this result in view of CUPID.

To optimize the light collection we also redesigned the LDs to fully cover the faces of the CUPID crystals. For the first time, we characterized the performances of quasi-square LDs coupled to LMO cubic crystals. We estimated and

demonstrated an improvement of the light collection of about 26% with respect to disk-shaped LDs, which have been tested in the same facility [58]. Moreover, the noise level achieved with the new LDs falls in the range of 35–70 eV which is well below the threshold required for CUPID (100 eV). This pushes at limits the particle identification capabilities for CUPID, which guarantee an α particles rejection higher than 99.9%.

Finally, we tested 2 possible configurations for the LD mounting. In the “baseline” CUPID configuration, LDs are spaced 0.5 mm and 4 mm from the bottom and top faces of the crystal respectively. We also tested a “gravity-assisted” configuration in which the top LD is leaned on the crystal. We eventually discarded the latter option as a viable solution for CUPID, since the gain in light collection is not worth the increased technical complexity of the assembly.

Acknowledgements The CUPID Collaboration thanks the directors and staff of the Laboratori Nazionali del Gran Sasso and the technical staff of our laboratories. This work was supported by the Istituto Nazionale di Fisica Nucleare (INFN); by the European Research Council (ERC) under the European Union Horizon 2020 program (H2020/2014–2020) with the ERC Advanced Grant no. 742345 (ERC-2016-ADG, project CROSS) and the Marie Skłodowska-Curie Grant Agreement no. 754496; by the Italian Ministry of University and Research (MIUR) through the grant Progetti di ricerca di Rilevante Interesse Nazionale (PRIN 2017, Grant no. 2017FJZMCJ); by the US National Science Foundation under Grant nos. NSF-PHY-1401832, NSF-PHY-1614611, and NSF-PHY-1913374. This material is also based upon work supported by the US Department of Energy (DOE) Office of Science under Contract nos. DE-AC02-05CH11231 and DE-AC02-06CH11357; and by the DOE Office of Science, Office of Nuclear Physics under Contract nos. DE-FG02-08ER41551, DE-SC0011091, DE-SC0012654, DE-SC0019316, DE-SC0019368, and DE-SC0020423. This work was also supported by the National Research Foundation of Ukraine under Grant no. 2020.02/0011. This research used resources of the National Energy Research Scientific Computing Center (NERSC). This work makes use of both the DIANA data analysis and APOLLO data acquisition software packages, which were developed by the CUORICINO, CUORE, LUCIFER and CUPID-0 Collaborations. The CUPID collaboration acknowledges the scientific and technical contributions from all collaborators. More information on the technical details of the experiments and the collaboration policies can be found at <https://cupid.lngs.infn.it>.

Data Availability Statement This manuscript has no associated data or the data will not be deposited. [Authors' comment: Data will be made available upon reasonable request.]

Open Access This article is licensed under a Creative Commons Attribution 4.0 International License, which permits use, sharing, adaptation, distribution and reproduction in any medium or format, as long as you give appropriate credit to the original author(s) and the source, provide a link to the Creative Commons licence, and indicate if changes were made. The images or other third party material in this article are included in the article's Creative Commons licence, unless indicated otherwise in a credit line to the material. If material is not included in the article's Creative Commons licence and your intended use is not permitted by statutory regulation or exceeds the permitted use, you will need to obtain permission directly from the copyright holder. To view a copy of this licence, visit <http://creativecommons.org/licenses/by/4.0/>.

Funded by SCOAP³. SCOAP³ supports the goals of the International Year of Basic Sciences for Sustainable Development.

References

1. M. Goeppert-Mayer, Phys. Rev. **48**, 512 (1935). <https://doi.org/10.1103/PhysRev.48.512>
2. A.S. Barabash, Universe **2020**(6), 159 (2020). <https://doi.org/10.3390/universe6100159>
3. O. Azzolini et al., Phys. Rev. D **100**, 092002 (2019). <https://doi.org/10.1103/PhysRevD.100.092002>
4. O. Azzolini et al., Phys. Rev. Lett. **123**, 262501 (2019). <https://doi.org/10.1103/PhysRevLett.123.262501>
5. J.B. Albert et al., Phys. Rev. D **93**, 072001 (2016). <https://doi.org/10.1103/PhysRevD.93.072001>
6. R. Arnold et al., Eur. Phys. J. C **79**(5), 440 (2019). <https://doi.org/10.1140/epjc/s10052-019-6948-4>
7. A. Gando et al., Phys. Rev. Lett. **122**, 192501 (2019). <https://doi.org/10.1103/PhysRevLett.122.192501>
8. A.S. Barabash et al., Phys. Rev. D **98**, 092007 (2018). <https://doi.org/10.1103/PhysRevD.98.092007>
9. E. Armengaud et al., Eur. Phys. J. C **80**(7), 674 (2020). <https://doi.org/10.1140/epjc/s10052-020-8203-4>
10. W. Furry, Phys. Rev. **56**, 1184 (1939). <https://doi.org/10.1103/PhysRev.56.1184>
11. H. Primakoff, S.P. Rosen, Rep. Prog. Phys. **22**(1), 121 (1959). <https://doi.org/10.1088/0034-4885/22/1/305>
12. M. Doi, T. Kotani, E. Takasugi, Prog. Theor. Phys. Suppl. **83**, 1 (1985). <https://doi.org/10.1143/PTPS.83.1>
13. R.N. Mohapatra, Phys. Rev. D **34**, 3457 (1986). <https://doi.org/10.1103/PhysRevD.34.3457>
14. J. Vergados, Phys. Rep. **133**(1), 1 (1986). [https://doi.org/10.1016/0370-1573\(86\)90088-8](https://doi.org/10.1016/0370-1573(86)90088-8)
15. F.F. Deppisch, M. Hirsch, H. Päs, J. Phys. G **39**, 124007 (2012). <https://doi.org/10.1088/0954-3899/39/12/124007>
16. S. Dell’Oro et al., Adv. High Energy Phys. **2016**, 2162659 (2016). <https://doi.org/10.1155/2016/2162659>
17. M. Fukugita, T. Yanagida, Phys. Lett. B **174**(1), 45 (1986). [https://doi.org/10.1016/0370-2693\(86\)91126-3](https://doi.org/10.1016/0370-2693(86)91126-3)
18. F.F. Deppisch, L. Graf, J. Harz, W.C. Huang, Phys. Rev. D **98**, 055029 (2018). <https://doi.org/10.1103/PhysRevD.98.055029>
19. R. Arnold et al., Phys. Rev. D **92**, 072011 (2015). <https://doi.org/10.1103/PhysRevD.92.072011>
20. A. Gando et al., Phys. Rev. Lett. **117**, 082503 (2016). <https://doi.org/10.1103/PhysRevLett.117.082503>
21. G. Anton et al., Phys. Rev. Lett. **123**, 161802 (2019). <https://doi.org/10.1103/PhysRevLett.123.161802>
22. M. Agostini et al., Science **365**(6460), 1445 (2019). <https://doi.org/10.1126/science.aav8613>
23. S.I. Alvis et al., Phys. Rev. C **100**, 025501 (2019). <https://doi.org/10.1103/PhysRevC.100.025501>
24. O. Azzolini et al., Phys. Rev. Lett. **123**, 032501 (2019). <https://doi.org/10.1103/PhysRevLett.123.032501>
25. D.Q. Adams et al., Phys. Rev. Lett. **124**, 122501 (2020). <https://doi.org/10.1103/PhysRevLett.124.122501>
26. M. Agostini et al., Phys. Rev. Lett. **125**, 252502 (2020). <https://doi.org/10.1103/PhysRevLett.125.252502>
27. E. Armengaud et al., Phys. Rev. Lett. **126**, 181802 (2021). <https://doi.org/10.1103/physrevlett.126.181802>
28. W. Armstrong, et al., (2019). [arXiv:1907.09376](https://arxiv.org/abs/1907.09376)
29. E. Fiorini, T.O. Niinikoski, Nucl. Instrum. Methods A **224**, 83 (1984)
30. S. Pirro, P. Mauskopf, Annu. Rev. Nucl. Part. Sci. **67**, 161 (2017)
31. D.Q. Adams, et al., (2021). [arXiv:2104.06906](https://arxiv.org/abs/2104.06906)

32. D.Q. Adams et al., Prog. Part. Nucl. Phys. **122**, 103902 (2022). <https://doi.org/10.1016/j.pnpnp.2021.103902>
33. C. Alduino et al., Phys. Rev. C **93**, 045503 (2016). <https://doi.org/10.1103/physrevc.93.045503>
34. C. Alduino et al., Eur. Phys. J. C **77**(8), 543 (2017). <https://doi.org/10.1140/epjc/s10052-017-5080-6>
35. V.I. Tretyak, Astropart. Phys. **33**(1), 40 (2010). <https://doi.org/10.1016/j.astropartphys.2009.11.002>
36. S. Rahaman et al., Phys. Lett. B **662**(2), 111 (2008). <https://doi.org/10.1016/j.physletb.2008.02.047>
37. J.W. Beeman et al., Astropart. Phys. **35**, 813 (2012). <https://doi.org/10.1016/j.astropartphys.2012.02.013>
38. J.W. Beeman et al., Eur. Phys. J. C **72**, 2142 (2012). <https://doi.org/10.1140/epjc/s10052-012-2142-7>
39. L. Cardani et al., J. Phys. G **41**, 075204 (2014). <https://doi.org/10.1088/0954-3899/41/7/075204>
40. J.W. Beeman et al., Adv. High Energy Phys. **2013**, 237973 (2013). <https://doi.org/10.1155/2013/237973>
41. J.W. Beeman et al., JINST **8**, P05021 (2013). <https://doi.org/10.1088/1748-0221/8/05/P05021>
42. L. Cardani et al., JINST **8**, P10002 (2013). <https://doi.org/10.1088/1748-0221/8/10/p10002>
43. D.R. Artusa et al., Eur. Phys. J. C **76**(7), 364 (2016). <https://doi.org/10.1140/epjc/s10052-016-4223-5>
44. O. Azzolini et al., Eur. Phys. J. C **78**(5), 428 (2018). <https://doi.org/10.1140/epjc/s10052-018-5896-8>
45. J. Beeman et al., Phys. Lett. B **710**(2), 318 (2012). <https://doi.org/10.1016/j.physletb.2012.03.009>
46. A. Barabash et al., Eur. Phys. J. C **74**(10), 3133 (2014). <https://doi.org/10.1140/epjc/s10052-014-3133-7>
47. E. Armengaud et al., JINST **10**, P05007 (2015). <https://doi.org/10.1088/1748-0221/10/05/P05007>
48. T.B. Bekker et al., Astropart. Phys. **72**, 38 (2016). <https://doi.org/10.1016/j.astropartphys.2015.06.002>
49. E. Armengaud et al., Eur. Phys. J. C **77**(11), 785 (2017). <https://doi.org/10.1140/epjc/s10052-017-5343-2>
50. V. Grigorieva et al., J. Mater. Sci. Eng. B **7**, 63 (2017). <https://doi.org/10.17265/2161-6221/2017.3-4.002>
51. D.V. Poda, AIP Conf. Proc. **1894**(1), 020017 (2017). <https://doi.org/10.1063/1.5007642>
52. V. Alenkov et al., Eur. Phys. J. C **79**(9), 791 (2019). <https://doi.org/10.1140/epjc/s10052-019-7279-1>
53. O. Azzolini et al., Eur. Phys. J. C **79**(7), 583 (2019). <https://doi.org/10.1140/epjc/s10052-019-7078-8>
54. O. Azzolini et al., Eur. Phys. J. C **78**(11), 888 (2018). <https://doi.org/10.1140/epjc/s10052-018-6340-9>
55. O. Azzolini et al., Eur. Phys. J. C **80**(8), 702 (2020). <https://doi.org/10.1140/epjc/s10052-020-8280-4>
56. E. Armengaud et al., Eur. Phys. J. C **80**(1), 44 (2020). <https://doi.org/10.1140/epjc/s10052-019-7578-6>
57. B. Schmidt et al., J. Phys. Conf. Ser. **1468**, 012129 (2020). <https://doi.org/10.1088/1742-6596/1468/1/012129>
58. A. Armato et al., Eur. Phys. J. C **81**, 104 (2021). <https://doi.org/10.1140/epjc/s10052-020-08809-8>
59. A. Armato et al., Phys. Rev. C **104**, 015501 (2021). <https://doi.org/10.1103/physrevc.104.015501>
60. A. Armato et al., JINST **16**, P02037 (2021). <https://doi.org/10.1088/1748-0221/16/02/p02037>
61. C. Alduino et al., JINST **11**, P07009 (2016). <https://doi.org/10.1088/1748-0221/11/07/P07009>
62. J.W. Beeman et al., JINST **8**, P07021 (2013). <https://doi.org/10.1088/1748-0221/8/07/p07021>
63. E.E. Haller, N.P. Palaio, W.L. Hansen, E. Kreysa, in *Neutron Transmutation Doping of Semiconductor Materials*. ed. by R.D. Larrabee (Plenum Press, New York, 1984), p.21
64. E. Andreotti et al., Nucl. Instrum. Methods A **664**(1), 161 (2012). <https://doi.org/10.1016/j.nima.2011.10.065>
65. M. Mancuso et al., EPJ Web Conf. **65**, 04003 (2014). <https://doi.org/10.1051/epjconf/20136504003>
66. D. Poda, Physics **3**(3), 473 (2021). <https://doi.org/10.3390/physics3030032>
67. M. Barucci et al., Nucl. Instrum. Methods A **935**, 150 (2019). <https://doi.org/10.1016/j.nima.2019.05.019>
68. C. Arnaboldi et al., JINST **13**(02), P02026 (2018). <https://doi.org/10.1088/1748-0221/13/02/p02026>
69. P. Carniti et al., Rev. Sci. Instr. **87**, 054706 (2016). <https://doi.org/10.1063/1.4948390>
70. C. Arnaboldi, G. Pessina, J. Low Temp. Phys. **151**(3), 964 (2008). <https://doi.org/10.1007/s10909-008-9785-7>
71. C. Arnaboldi et al., Rev. Sci. Instrum. **86**(12), 124703 (2015). <https://doi.org/10.1063/1.4936269>
72. C. Arnaboldi et al., Nucl. Instrum. Methods A **617**(1–3), 327 (2010). <https://doi.org/10.1016/j.nima.2009.09.023>
73. C. Arnaboldi et al., Nucl. Instrum. Methods A **520**, 578 (2004). <https://doi.org/10.1016/j.nima.2003.11.319>
74. C. Arnaboldi et al., IEEE Trans. Nucl. Sci. **49**(5), 2440 (2002). <https://doi.org/10.1109/TNS.2002.803886>
75. S.D. Domizio et al., JINST **13**, P12003 (2018). <https://doi.org/10.1088/1748-0221/13/12/p12003>
76. A. Branca, J. Phys. Conf. Ser. **1468**(1), 012118 (2020). <https://doi.org/10.1088/1742-6596/1468/1/012118>
77. O. Azzolini et al., Eur. Phys. J. C **78**(9), 734 (2018). <https://doi.org/10.1140/epjc/s10052-018-6202-5>
78. E. Andreotti et al., Astropart. Phys. **34**(11), 822 (2011). <https://doi.org/10.1016/j.astropartphys.2011.02.002>
79. V. Radeka, N. Karlovac, Nucl. Instrum. Methods A **52**, 86 (1967). [https://doi.org/10.1016/0029-554X\(67\)90561-7](https://doi.org/10.1016/0029-554X(67)90561-7)
80. E. Gatti, P.F. Manfredi, Riv. Nuovo Cimento **9**, 1 (1986). <https://doi.org/10.1007/BF02822156>
81. G. Buse et al., Nucl. Instrum. Methods A **891**, 87 (2018). <https://doi.org/10.1016/j.nima.2018.02.101>
82. C. Arnaboldi et al., Astropart. Phys. **34**(11), 797 (2011). <https://doi.org/10.1016/j.astropartphys.2011.02.006>